

TFEC-2024-50704

SUBGRID MODELING OF REACTION-RATE USING A MULTI-SCALE STRATEGY FOR LARGE-EDDY SIMULATION OF TURBULENT COMBUSTION

R. Smith, 1,* T. Elliott, 1 R. Ranjan 1

¹Department of Mechanical Engineering, The University of Tennessee at Chattanooga 615 McCallie Ave, Chattanooga, TN, USA 37403

ABSTRACT

In this study, we examine the performance of a multi-scale model for large-eddy simulation (LES) of turbulent combustion. The model referred to as RRLES performs the closure of the filtered reaction-rate term in the species transport equation while performing LES by using the linear eddy mixing (LEM) model. The RRLES model uses a multi-scale strategy to obtain the filtered reaction rate of the species and has been shown to address some of the challenges associated with the well-established LEMLES approach. The originally proposed RRLES strategy used a multilevel adaptive mesh refinement (AMR) framework, which was extended to use a single grid-based strategy to enable the application to complex geometries. Additionally, a local dual-resolution grid strategy has also been developed and can potentially be used with different grid topologies, without the need for the AMR. We assess the accuracy and efficiency of the single and dual-grid RRLES approaches by considering a freely propagating turbulent premixed flame under two different initial conditions corresponding to the thin reaction zone (TRZ) and the broken/distributed reaction zone (B/DRZ) regimes.

KEY WORDS: Large-eddy simulation, linear-eddy mixing model, turbulent premixed flame

1. INTRODUCTION

Numerical investigation of turbulent flames can be performed using approaches with different levels of fidelity. For example, direct numerical simulation (DNS), where all the relevant scales are captured, is typically used for the investigation of fundamental features of turbulence-chemistry interaction [1, 26, 29, 33, 35]. However, the large computational cost of DNS limits its usage to simplified geometries and lower-to-moderate Reynolds number (*Re*) flows. Large-eddy simulation (LES), on the other hand, appears to be a viable alternative for the simulation of practically relevant flows, where the large scales are resolved, and the subgrid-scale (SGS) effects are modeled. A major focus of turbulent combustion modeling is on the closure of the filtered reaction-rate term in the governing equations [24]. Although there exists a wide range of SGS models for turbulent combustion, there are challenges in terms of their regime of applicability, the ability to account for finite-rate kinetics effects, handling of different modes of turbulent combustion (premixed and non-premixed), etc. These challenges have lead to the development of numerous SGS closures such as partially stirred reactor (PaSR) [8], thickened flame model (TFM) [4], flame surface density (FSD) [2], conditional moment closure (CMC) [15], conditional source estimation (CSE) [32], transported probability density function (TPDF) [5, 9], multi-environment PDF (MEPDF) [7], one-dimensional turbulence (ODT) [6], and linear-eddy model (LEM) [18, 20] and its variants [22, 28], etc. Here, we focus on the assessment of a multi-scale model for LES,

^{*}Corresponding R. Smith: nbh188@mocs.utc.edu

referred to as RRLES where the subgrid reaction-rate closure is attained using LEM.

The RRLES approach [28] is a modification of the well-known LEMLES approach [18], a multi-scale strategy that is used to obtain the filtered reaction rate term. The filtered LES equations are evolved on the 3D grid and at every LES time step, the filtered species mass fractions and the filtered temperature fields are used to reconstruct SGS variation on the 1D notional LEM domain inside each LES cell. After solving for the subgrid reaction-diffusion equation and including the effect of turbulent mixing on the 1D LEM domain, the filtered reaction rates are computed and projected back to the 3D grid. The originally proposed RRLES strategy used a multilevel adaptive mesh refinement (AMR) framework. The approach was extended to use a single grid-based strategy to enable the application to complex geometries [22]. Recently, a local dual grid-based strategy has also been developed, which can potentially be used with different grid topologies, without the need for an AMR [27]. In the present study, we focus on the assessment of the single- and dual-grid approaches for the simulation of turbulent premixed flames.

We consider two temporally evolving methane/air flames with one pertaining to the thin reaction zone (TRZ) regime and the other to the broken/distributed reaction zone (B/DRZ) regime. Note that turbulent premixed flames can be classified into wrinkled flamelets (WF), corrugated flamelets (CF), thin reaction zone (TRZ), and broken/distributed reaction zone (B/DRZ) [23, 25] regimes based on the length- and velocity-scale ratios corresponding to turbulence and laminar flame properties. In general, the simulation of practically relevant TRZ and B/DRZ flames is considered challenging, and therefore, is considered here for the model evaluation.

This article is arranged as follows. The next section describes the governing equations and the subgrid closure formulations that are considered in this study. The numerical methodology and problem description are presented after that. The following section presents the discussion of results. Finally, the outcomes of this study are summarized.

2. MATHEMATICAL FORMULATION

In this section, we first describe the governing equations. Afterward, we describe the SGS closure models employed in this study.

2.1 Governing equations

The compressible LES equations are obtained by spatially filtering the Navier–Stokes equations using a tophat Favre filter, appropriate for finite volume schemes [34]. Here, \overline{f} is the spatially filtered quantity for a field variable f, and $\widetilde{f} = \overline{\rho f}/\overline{\rho}$ is the Favre-filtered quantity where ρ represents the density. The filtered LES equations can be written as:

$$\frac{\partial \overline{\rho}}{\partial t} + \frac{\partial \overline{\rho} \widetilde{u}_i}{\partial x_i} = 0, \tag{1}$$

$$\frac{\partial \overline{\rho} \widetilde{u}_i}{\partial t} + \frac{\partial}{\partial x_i} [\overline{\rho} \widetilde{u}_i \widetilde{u}_j + \overline{P} \delta_{ij} - \overline{\tau}_{ij} + \tau_{ij}^{sgs}] = 0, \tag{2}$$

$$\frac{\partial \overline{\rho}\widetilde{E}}{\partial t} + \frac{\partial}{\partial x_i} [(\overline{\rho}\widetilde{E} + \overline{P})\widetilde{u}_i + \overline{q}_i - \widetilde{u}_j \overline{\tau}_{ij} + H_i^{sgs} + \sigma_i^{sgs}] = 0, \tag{3}$$

$$\frac{\partial \overline{\rho} \widetilde{Y}_k}{\partial t} + \frac{\partial}{\partial x_i} [\overline{\rho} (\widetilde{Y}_k \overline{u_i} + \widetilde{Y}_k \widetilde{V}_{i,k}) + y_{i,k}^{sgs} + \theta_{i,k}^{sgs}] = \overline{\dot{\omega}}_k \qquad k = 1, ..., N_s.$$
 (4)

Here, ρ is the density, $(u_i)_{i=1,2,3}$ is the velocity vector in Cartesian coordinates, T is the temperature, P is the pressure, and Y_k is the mass fraction for the k^{th} species. Additionally, N_s is the total number of species in the flow. The total energy in the system is the sum of the internal energy and the kinetic energy. As a result, the filtered total energy is presented as a sum of the filtered internal energy (\widetilde{e}) , the resolved kinetic energy $(\frac{1}{2}[\widetilde{u}_i\widetilde{u}_j])$, and the subgrid kinetic energy $(k^{sgs} = \frac{1}{2}[\widetilde{u}_i\widetilde{u}_i - \widetilde{u}_i\widetilde{u}_i])$. The thermally perfect gas equation of state is used to close the equations as $\overline{P} = \overline{\rho}(\widetilde{R}\widetilde{T} + T^{sgs})$. The filtered viscous stress tensor and the filtered heat-flux vector are approximated as:

$$\overline{\tau}_{ij} = 2\mu(\widetilde{T})(\widetilde{S}_{ij} - \frac{1}{3}\widetilde{S}_{kk}\delta_{ij}),\tag{5}$$

$$\overline{q}_{i} = -k(\widetilde{T})\frac{\partial \widetilde{T}}{\partial x_{i}} + \overline{\rho} \sum_{k=1}^{N_{s}} \widetilde{h}_{k} \widetilde{Y}_{k} \widetilde{V}_{i,k} + \sum_{k=1}^{N_{s}} q_{i,k}^{sgs},$$

$$\tag{6}$$

where $\widetilde{S}_{ij} = \frac{1}{2} (\frac{\partial \widetilde{u}_i}{\partial x_j} + \frac{\partial \widetilde{u}_j}{\partial x_i})$ is the resolved rate of strain. The filtered diffusion velocity for the k^{th} species is modeled as

$$\widetilde{V}_{i,k} = -\overline{D}_k \frac{\partial \widetilde{X}_k}{\partial x_i} + \frac{1}{W} \sum_{k=1}^{N_s} \overline{D}_k W_k \frac{\partial X_k}{\partial x_i}, \tag{7}$$

where W is the mixture molecular weight, and \overline{D}_k and \widetilde{X}_k are the diffusion coefficient and mole fraction of the k_{th} species, respectively. The diffusion coefficient for a species is obtained through the well known mixture-averaged formulation [25].

All of the subgrid-scale terms, denoted with a "sgs" superscript, are unclosed, and therefore, require specific modeling. These terms are:

$$\tau_{ij}^{sgs} = \overline{\rho}(\widetilde{u_i u_j} - \widetilde{u}_i \widetilde{u_j}), \tag{8}$$

$$H_i^{sgs} = \overline{\rho}(\widetilde{Eu}_i - \widetilde{E}\widetilde{u}_i) + (\overline{u_iP} - \widetilde{u}_i\overline{P}), \tag{9}$$

$$\sigma_i^{sgs} = (\overline{u_j \tau_{ij}} - \widetilde{u}_j \overline{\tau}_{ij}), \tag{10}$$

$$y_{i,k}^{sgs} = \overline{\rho}(\widetilde{u_i Y_k} - \widetilde{u}_i \widetilde{Y}_k), \tag{11}$$

$$\theta_{i,k}^{sgs} = \overline{\rho}(\widetilde{Y_k V_{i,k}} - \widetilde{Y_k V_{i,k}}), \tag{12}$$

$$q_{i,k}^{sgs} = \overline{\rho}(h_k \widetilde{Y_k V}_{i,k} - \widetilde{h}_k \widetilde{Y}_k \widetilde{V}_{i,k}), \tag{13}$$

$$T^{sgs} = \widetilde{RT} - \widetilde{R}\widetilde{T},\tag{14}$$

$$E_k^{sgs} = Y_k(\widetilde{T})e_k - \widetilde{Y}_k(\widetilde{T})e_k, \tag{15}$$

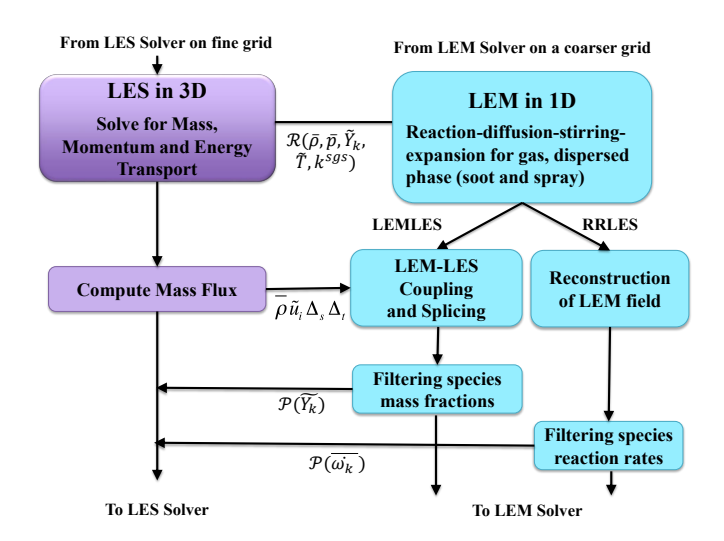


Fig. 1 A typical workflow in the LEMLES and RRLES strategies [28].

The governing equations are complete after specifying closure models for the SGS terms, and initial and boundary conditions for the specific problem. Next, we briefly describe the subgrid models.

2.2 Subgrid Modeling of SGS Stress and Scalar Flux

The subgrid stress and enthalpy flux and the subgrid viscous work terms are present even in non-reacting flows, and their modeling follows past effort relying on eddy viscosity formulation [19]. The unclosed subgrid stress term τ_{ij}^{sgs} is modeled as

$$\tau_{ij}^{sgs} = -2\overline{\rho}\nu_t(\widetilde{S}_{ij} - \frac{1}{3}\widetilde{S}_{kk}\delta_{ij}) + \frac{2}{3}k^{sgs}\delta_{ij},\tag{16}$$

and the two unclosed terms in the energy equation, H_i^{sgs} and σ_i^{sgs} , are modeled together:

$$H_i^{sgs} + \sigma_i^{sgs} = (\overline{\rho} \nu_t \mu) \frac{\partial k^{sgs}}{\partial x_i} + \frac{\overline{\rho} \nu_t c_p}{P r_t} \frac{\partial \widetilde{T}}{\partial x_i} + \widetilde{u}_j \tau_{ij}^{sgs}. \tag{17}$$

Here we employ a one-equation model for the subgrid kinetic energy [13, 19] to determine the subgrid eddy viscosity as $v_t = C_v \sqrt{k^{sgs}} \Delta$, where Δ is the grid filter width and C_v is a coefficient calculated using the localized dynamic kinetic energy model (LDKM) [10, 13].

2.3 Subgrid Modeling of Filtered Reaction Rate

The RRLES approach [28] is a modification of the well-known LEMLES approach [18], where the filtered reaction-rate terms $(\overline{\dot{\omega}}_i)$ are modeled using a multi-scale LEM framework. At every LES time step, the filtered species mass fractions (\tilde{Y}_i) and the filtered temperature (\tilde{T}) evolving at the resolved level are used to reconstruct SGS variation on the 1D notional LEM domain inside each LES cell, and after solving for the subgrid reaction-diffusion equation and including the effect of turbulent mixing on the LEM domain, the filtered reaction rates are computed and projected back to the LES grid. A workflow of the RRLES strategy compared to LEMLES is shown in Fig. 1.

The first step is the reconstruction of the species mass fraction and the temperature field in the 1D LEM domain, which is performed as

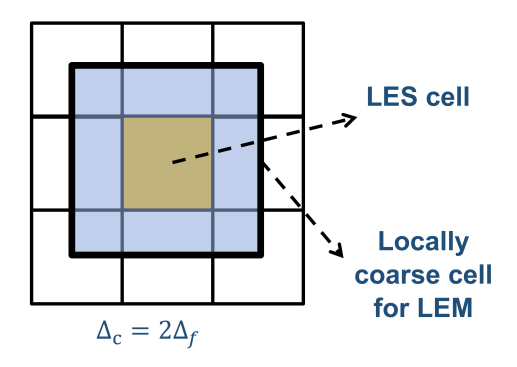


Fig. 2 Schematic of the dual-grid strategy employed in the RRLES approach.

$$Y_i^{\text{LEM}}(s) = \mathcal{R}\left(\widetilde{Y}_i, \nabla \widetilde{Y}_i\right), \quad T^{\text{LEM}}(s) = \mathcal{R}\left(\widetilde{T}, \nabla \widetilde{T}\right),$$
 (18)

where, $\mathcal{R}\left(\widetilde{\varphi}, \nabla\widetilde{\varphi}\right) = \widetilde{\varphi} - \nabla\widetilde{\varphi}\Delta/2 + |\nabla\widetilde{\varphi}|\Delta s$ is a gradient-based reconstruction operator, 's' represents the co-ordinate along the 1D LEM domain, and Δ represents the LES filter size. After the reconstruction step, the governing equations for the species mass-fraction and the temperature are solved on the notional 1D LEM domain inside each LES computational cell as

$$\rho \frac{\partial Y_i}{\partial t} = F_{i,\text{stir}} - \frac{\partial}{\partial s} \left(\rho Y_i V_{s,i} \right) + \dot{\omega}_i, \tag{19}$$

$$\rho C_{p,\text{mix}} \frac{\partial T}{\partial t} = F_{T,\text{stir}} + \frac{\partial}{\partial s} \left(\kappa \frac{\partial T}{\partial s} \right) - \frac{\partial}{\partial s} \left(\sum_{i=1}^{N_S} h_i \rho Y_i V_{s,i} \right) - \sum_{i=1}^{N_S} h_i \dot{\omega}_i. \tag{20}$$

Each 1D LEM domain is discretized using $N_{\rm LEM}$ cells to ensure the required spatial resolution of the scalar fields. The processes involved in the subgrid evolution include molecular diffusion, turbulent transport by the unresolved eddies, chemical reaction, and thermal expansion for the species at their respective spatial and temporal scales. The terms $F_{k,\rm stir}$ and $F_{T,\rm stir}$ represent the stochastic events, which simulate the effects of turbulent mixing by the SGS eddies on the 1D LEM lines [12, 18]. Finally, after solving for the SGS variations, the filtered reaction-rate term $\dot{\omega}_i$ is obtained for the corresponding LES cell through:

$$\overline{\dot{\omega}}_i = \frac{\sum_{m=1}^{N_{\text{LEM}}} \dot{\omega}_{i,m} \Delta V_m}{\sum_{m=1}^{N_{\text{LEM}}} \Delta V_m}.$$
(21)

The approach was extended to use a single grid-based strategy to enable the application to complex geometries [22]. Recently, a local dual grid-based strategy has also been developed, which can potentially be used with different grid topologies, without the need for an AMR [27]. We will assess the performance of both these approaches.

A schematic of the local dual-grid strategy is shown in Fig. 2. In this strategy, the LEM subgrid fields evolve on a coarser LES grid with resolution $\Delta^{LEM}=2\Delta$, while the LES governing equations are still resolved on the much finer grid of resolution Δ . The coarser grid has more unresolved scales and its use leads to an improved prediction by solving the subgrid LEM equations. Additionally, this strategy requires consistent restriction operations for the resolved LES quantities needed by LEM. When compared to the single grid-based strategy, the dual-grid strategy has the advantage in that the estimate for the SGS variation in the 1D LEM (at Δ^{LEM}) can be constructed from the solution on the finer LES grid.

Table 1 Initial turbulent premixed flame parameters

Case	Closure	$\mathbf{N_x} imes \mathbf{N_y} imes \mathbf{N_z}$	$\mathbf{u}'/\mathbf{S_L}$	$1/\delta_{\mathbf{L}}$	Re	Ka	Da
A_1	DNS	$192 \times 192 \times 192$	10.0	0.74	62.8	12.6	0.63
A_2	LEMLES	$64 \times 64 \times 64$	10.0	0.74	62.8	12.6	0.63
A_3	RRLES	$96 \times 96 \times 96$	10.0	0.74	62.8	12.6	0.63
A_4	DUAL-RRLES	$64 \times 64 \times 64$	10.0	0.74	62.8	12.6	0.63
B_1	DNS	$256 \times 256 \times 256$	50.0	6.2	478.7	113.9	0.19
B_2	LEMLES	$96 \times 96 \times 96$	50.0	6.2	478.7	113.9	0.19
B_3	RRLES	$96 \times 96 \times 96$	50.0	6.2	478.7	113.9	0.19
B_4	DUAL-RRLES	$96 \times 96 \times 96$	50.0	6.2	478.7	113.9	0.19

3. COMPUTATIONAL SETUP AND APPROACH

In this section the details of the numerical methodology and the computational setup for both premixed and non-premixed cases are discussed.

3.1 Numerical methodology

The governing equations described in Sec. 2.1 are solved using a well-established three-dimensional (3D) parallel, multi-species compressible reacting flow solver, referred to as AVF-LESLIE [14, 30]. It is a multi-physics simulation tool capable of performing DNS and LES of reacting/non-reacting flows in canonical and moderately complex flow configurations. It has been extensively used in the past to study a wide variety of flow conditions, including acoustic flame-vortex interaction, premixed flame turbulence interaction, non-premixed combustion, and compressible turbulence [3, 14, 16, 30, 36].

The solver utilizes a finite volume-based spatial discretization of the governing equations in their conservative form on a structured grid using the generalized curvilinear coordinates. The spatial discretization is based on the well-known second-order accurate MacCormack scheme [17]. The time integration of the semi-discrete system of equations is performed by an explicit second-order accurate scheme. The solver can handle arbitrarily complex finite-rate chemical kinetics. The mixture-averaged transport properties, the finite-rate kinetics source terms, and the thermally perfect gas-based thermodynamic properties are obtained using the Cantera software [11]. The parallelization of the solver is based on the standard domain decomposition technique based on the message-passing interface library.

3.2 Computational setup

The test cases correspond to the interaction of an initially premixed laminar flame with a decaying isotropic turbulence. Figure 3a shows a schematic of the premixed planar flame configuration. The initial flame front is specified near the center of the computational domain with reactants and products on its left and right sides, respectively. The extent of the computational domain is $L_x \times L_y \times L_z$ in the streamwise, transverse, and spanwise directions, where L=0.0055 m. The flow field is initialized using an isotropic turbulent flow field and is superimposed with a one-dimensional planar flame solution obtained at $\phi=0.8$, $T_{ref}=570$ K, and $P_{ref}=1$ atm. Here, ϕ denotes the equivalence ratio of the methane-air mixture, T_{ref} is the temperature on the reactants side, and P_{ref} is the reference pressure. These conditions are based on past studies, which are typical of many practical application devices [21, 29]. A characteristic-based inflow-outflow boundary condition is used in the streamwise direction and a periodic boundary condition is used along the spanwise and transverse directions.

The simulation parameters for all of the cases are presented in Table 1. Here l is the integral length scale, u' is the turbulence intensity, S_L is the laminar flame speed, $\delta = v/S_L$ is the Zeldovich flame thickness, and Re, Ka, and Da are the integral Reynolds number, the Karlovitz number, and the Damköhler number, which

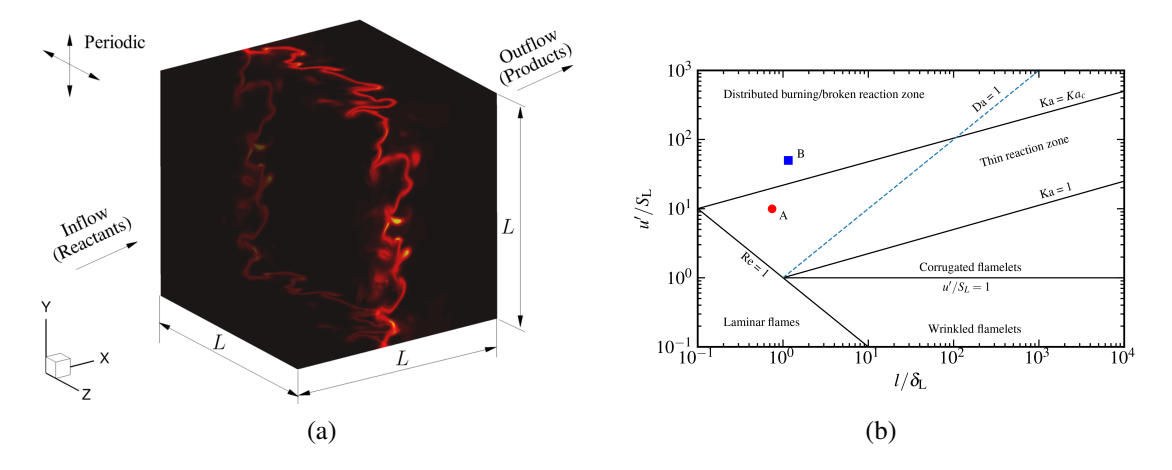


Fig. 3 A schematic of the turbulent premixed flame configuration (a) and the premixed flame regime diagram [23] (b) showing the cases considered in the present study.

are defined as $Re=\frac{u'l}{v}$, $Ka=\sqrt{\frac{u'^3\delta}{S_L^3l}}$ and $Da=\frac{S_Ll}{u'\delta}$, respectively. We conduct four simulations employing DNS, LEMLES, RRLES, and dual-grid RRLES for each of the two flames. The cases corresponding to the TRZ regime are labeled as Case A_m where the subscript "m" corresponds to the different closure methods. Similarly, the cases corresponding to the B/DRZ regime are labeled as Case B_m . The flames are estimated to be in their respective regimes based on initial conditions and are indicated in Fig. 3b.

The grid resolution is chosen based on previous studies, and for the conditions considered here is more than sufficient to reach $k_{\text{max}}\eta \geq 1$ for DNS, where k_{max} is the largest wave number and η is the Kolmogorov length scale. Specifically, $k_{max}\eta = 7.23$ and 2.1 for Cases A_{1-4} and B_{1-4} , respectively. With the grids employed in the present study, it is estimated that the thermal flame thickness, $\delta_L = (T_b - T_u)/|\nabla T|_{max}$, is resolved by around by 20 points in DNS and 5 points in LES. The simulations are carried out long enough to allow flame-turbulence interaction to properly evolve and all the results are compared after three initial eddy turnover times where $t_0 = l/u'$ is the initial eddy turnover time.

4. RESULTS AND DISCUSSION

In this section we first compare the flame structure and its statistics predicted by different closures and then assess the ability of various closures to capture the SGS effects on the flame-turbulence interactions.

4.1 Structural features of flames

The flame structure and its characteristics are assessed using a progress variable c, which is defined based on the mass fraction of the fuel as

$$c = \frac{Y_{CH_4,u} - Y_{CH_4}}{Y_{CH_4,u} - Y_{CH_4,b}} \tag{22}$$

where Y_{CH_4} denotes the mass fraction of methane, and subscripts "u" and "b" denote its value in the unburned reactants and the burned products sides, respectively. The value of c ranges from 0 in the fresh reactants to 1 in the burned products. Just as in past studies [30, 31], we identify a notional flame surface by an iso-level of c = 0.8 and the bounds of the flame brush correspond to $c \in [0.01, 0.99]$. While comparing LEMLES and RRLES predictions, the filtered progress variable \tilde{c} is defined in a way similar to Eq. 22 but using the filtered mass fraction of the fuel.

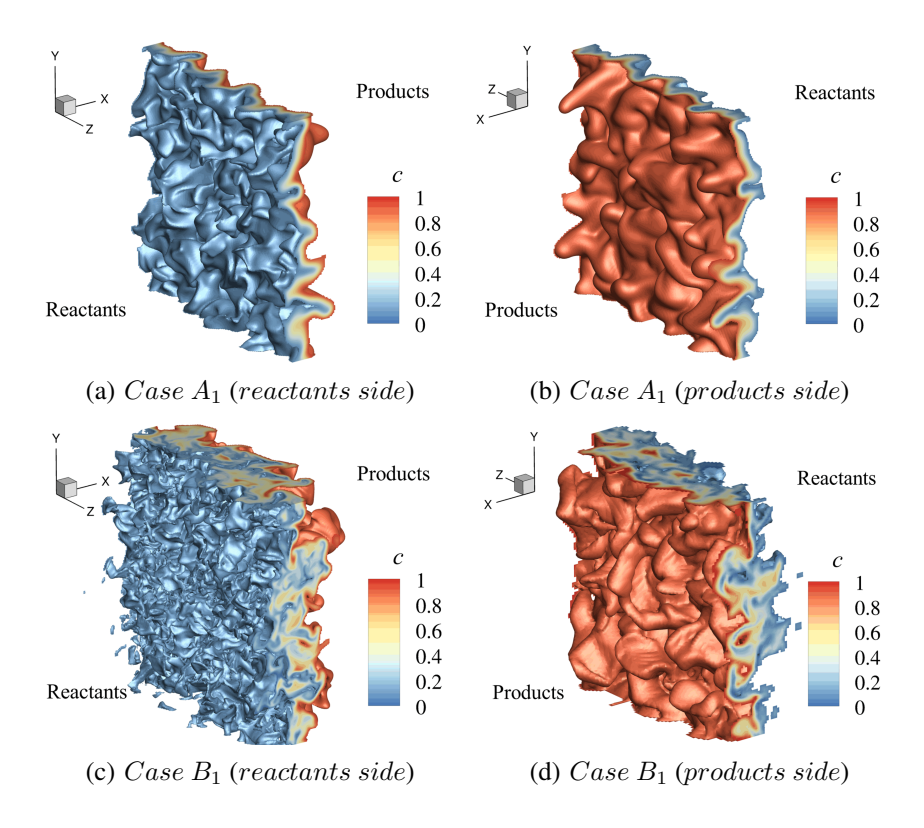


Fig. 4 Structure of the flame brush for the two premixed flames obtained using DNS.

Figure 4 shows the instantaneous structure of the flame brush obtained from DNS for the three flames. Here we can observe intense wrinkling and stretching of the initially planar flame surface by the turbulent eddies. The effect of heat release and associated thermal expansion across the flame is apparent in terms of an increase in the overall length scales associated with the protruding structures on both the reactants and the products sides. Typically, turbulent eddies sustain the flame by transporting pockets of cold reactants toward the reaction zone. As expected, the flame structure is continuous, thus preventing any local extinction. The width of the flame brush varies spatially, due to the straining effect of the large-scale eddies, and the increased flame surface area results in an increased fuel consumption rate [25, 30, 37].

Figure 5 compares the flame structure from three of the four simulated cases. The wrinkling and stretching of the flame are predicted by all closures in a consistent manner. All simulations show a continuous flame structure and no sign of local extinction for these conditions. It is to be noted that there are noticeable qualitative differences between the employed closures. Specifically, DNS and RRLES show more fine-grained features compared to LEMLES, which is especially apparent in Case B. Additionally, the LEMLES results for the scalar field differs from the other formulations due to its multi-scale nature, as the LEMLES-based resolved scalar field corresponds to the resolved value of the corresponding LEM field on the LES grid, whereas in the RRLES formulation the resolved scalar field is explicitly solved.

4.2 Flame statictics

The global flame structure is examined in terms of the spatially averaged quantities, where the spatial averaging of a quantity q is performed along the homogeneous y- and z-directions through

$$\langle q \rangle(x,t) \equiv \frac{1}{L^2} \int_0^L \int_0^L q(x,y,z,t) \, dy \, dz. \tag{23}$$

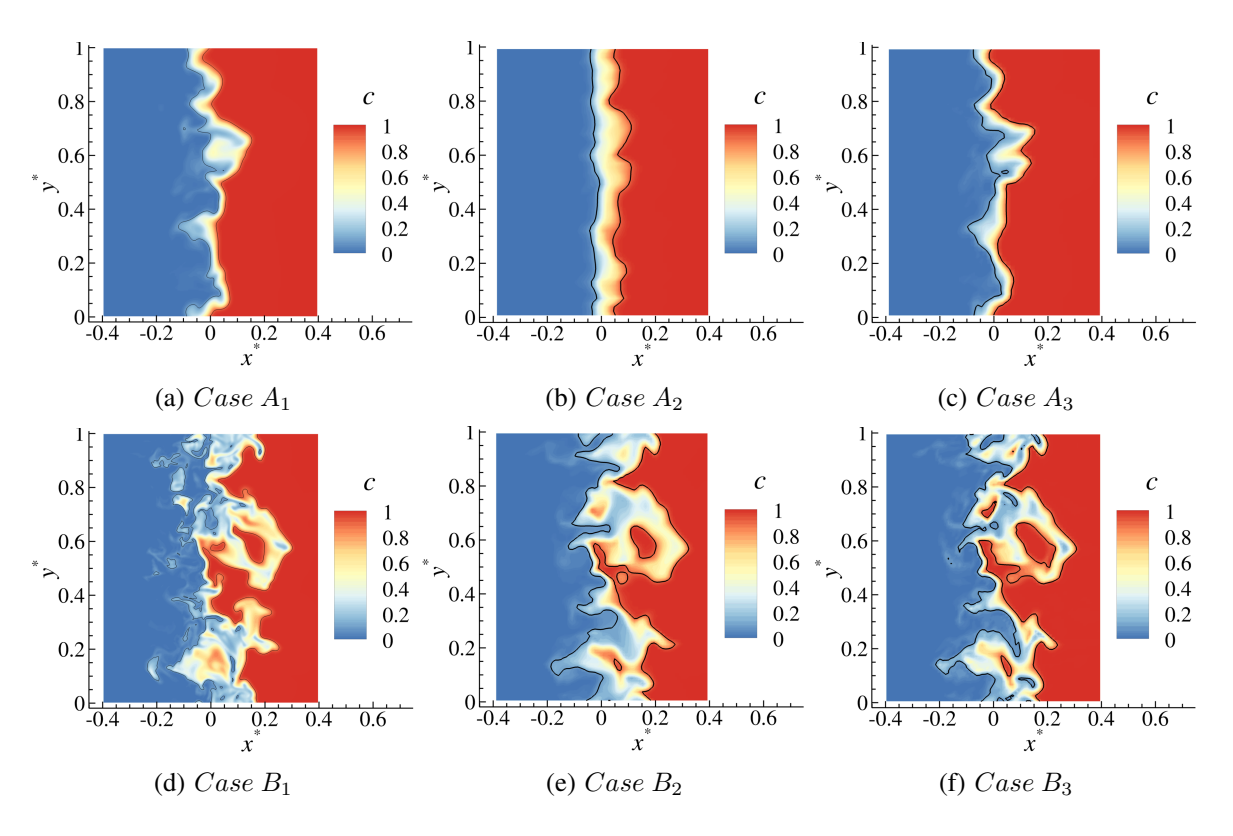


Fig. 5 Contours of filtered temperature field overlaid with the flame brush extents in the central x - y plane identified using the filtered progress variable.

The streamwise profile of the spatially averaged quantities for all premixed cases at $t=3t_0$ is presented in Fig. 6. In all the cases, we observe a good agreement of the results with the DNS data, and all the methods are able to capture the global flame structure. RRLES shows an overall good agreement with the DNS results for the cases, implying that the blending employed by the formulation allows it to include contribution from LEM at the subgrid level as the turbulence level increases and with a decrease in turbulence level it takes contributions from the quasi-laminar chemistry. In Case A with a lower value of Ka, LEMLES greatly underpredicts the heat release rate and product mass fraction. At a higher value of Ka (Case B), we observe slight under-prediction by LEMLES, but the overall flame structure compares well with the other closure methods.

Figure 7 shows the streamwise profile of the conditionally averaged quantities, which include temperature, heat release rate, and mass fraction of product species (H₂). Similar to the spatially averaged profile, the asymptotic behavior of the RRLES closure is evident here, as we can observe that its prediction approaches DNS when the turbulence level is relatively small (Case A). Here we again see evidence of the limitations of the LEMLES formulation in Case A when the local flow conditions have a low subgrid-scale turbulence.

4.3 Single- and dual-grid strategy comparison

A direct comparison of the spatially averaged quantities for single- and dual-grid RRLES of Case A is presented in Fig. 8. Figure 9 shows the conditionally averaged quantities.

5. SUMMARY

Numerical investigations of subgrid-scale dynamics of premixed flame interaction with decaying isotropic turbulence are carried out using single- and dual-grid RRLES strategies. We consider two premixed flames

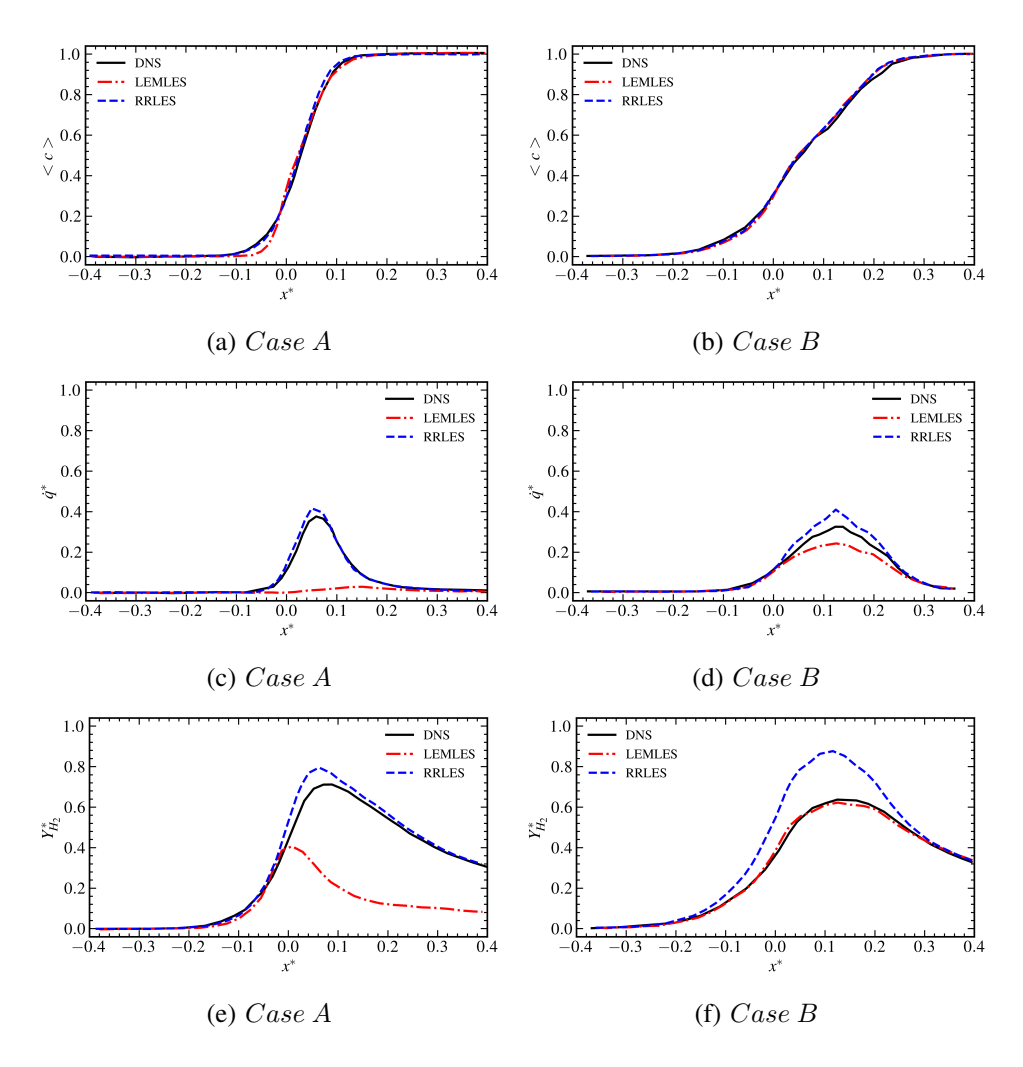


Fig. 6 Streamwise profile of the spatially averaged scaled progress variable, heat release rate, and product mass fraction.

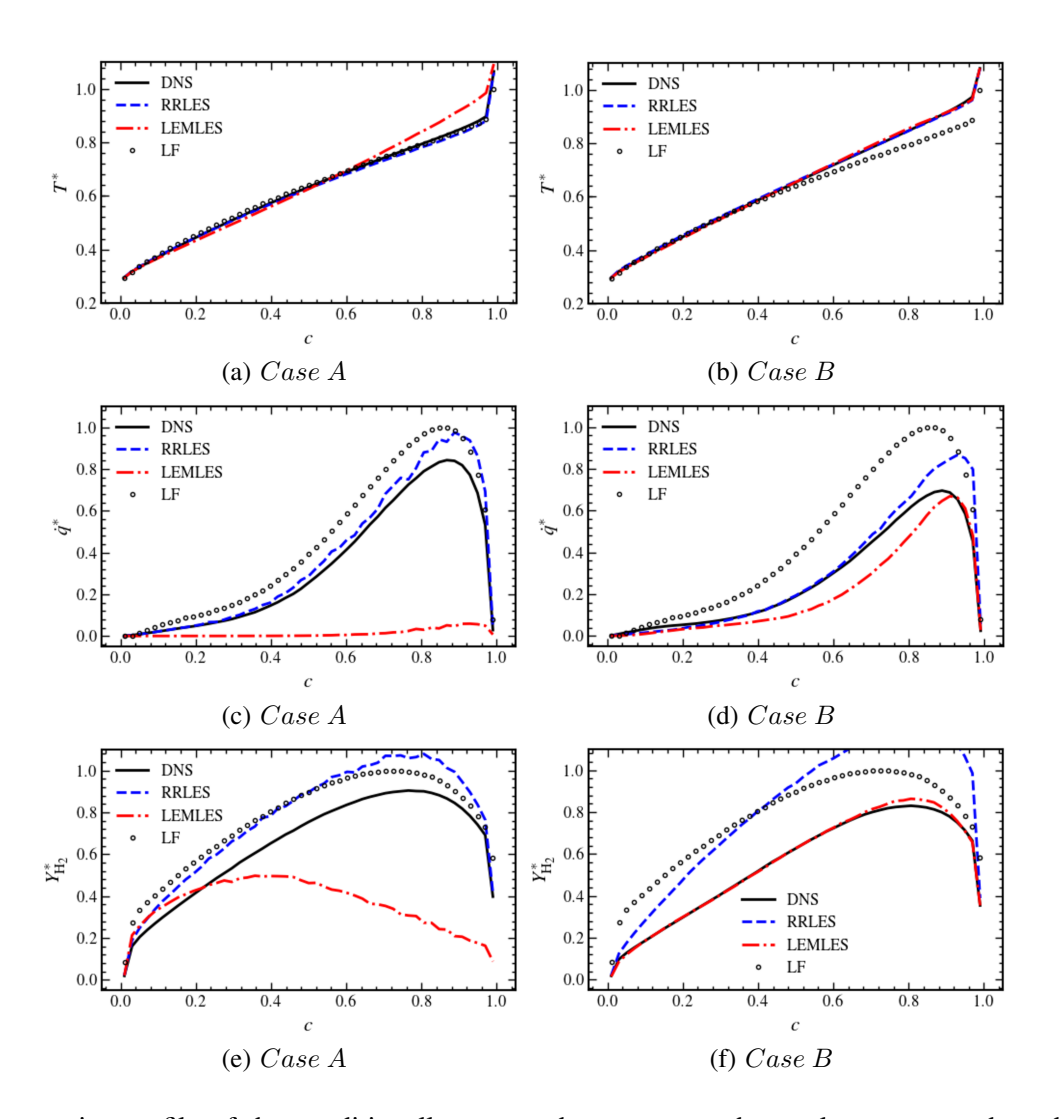


Fig. 7 Streamwise profile of the conditionally averaged temperature, heat release rate, and product mass fraction.

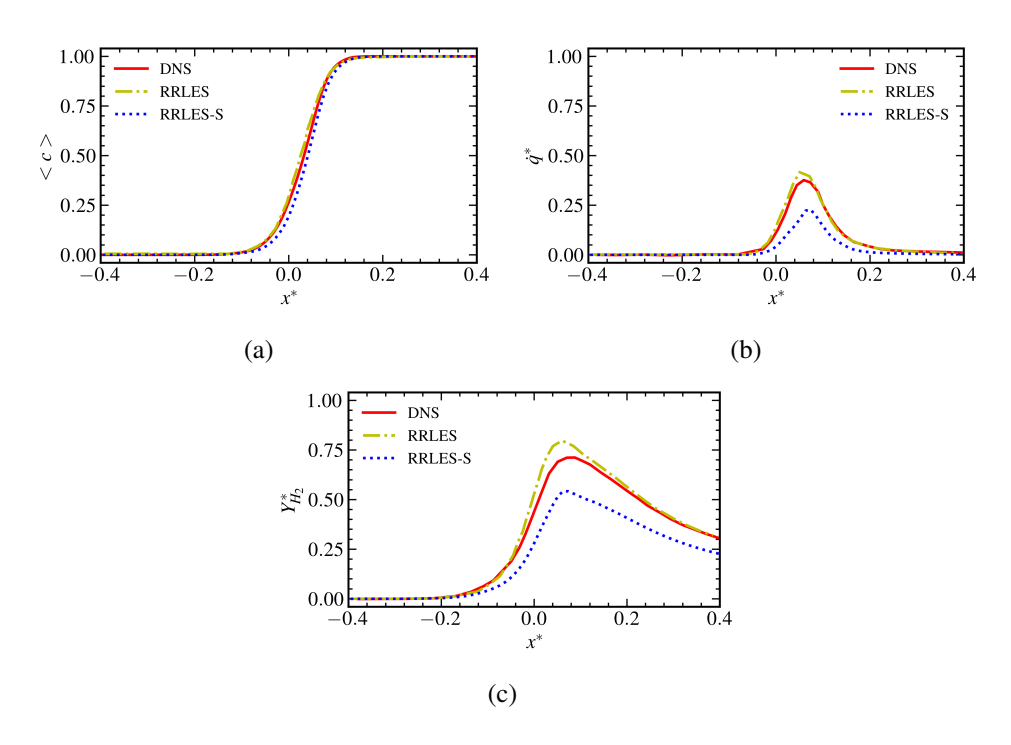


Fig. 8 Streamwise profile of the spatially averaged scaled progress variable (a), heat release rate (b), and product mass fraction (c) for single- and dual-grid RRLES of the TRZ flame.

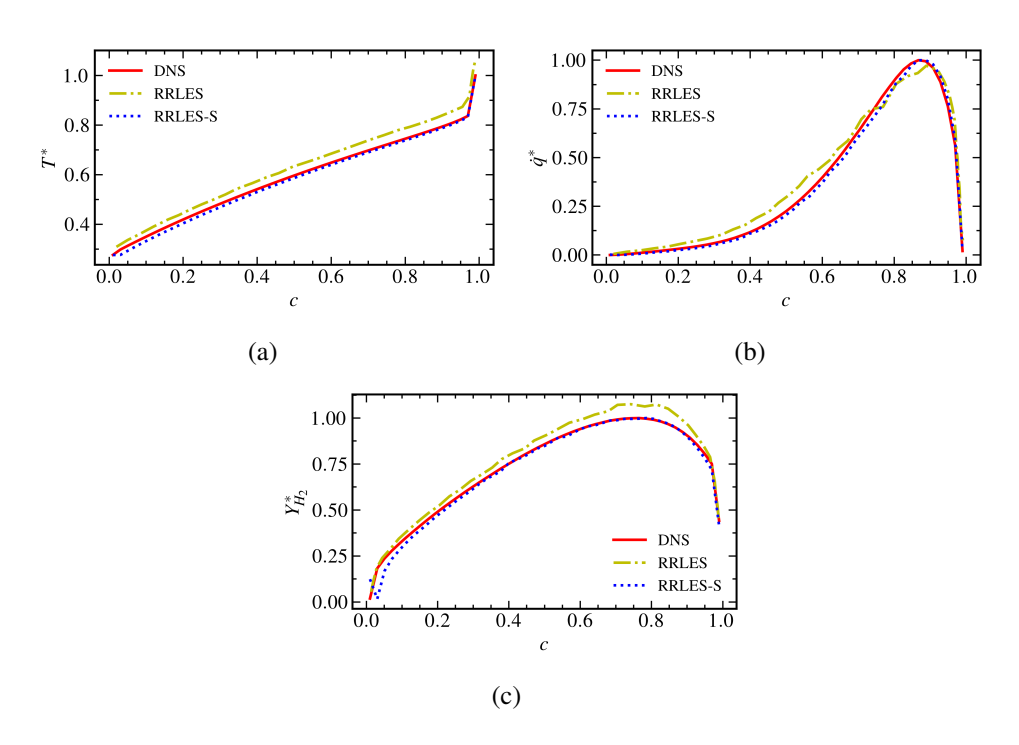


Fig. 9 Streamwise profile of the conditionally averaged temperature (a), heat release rate (b), and product mass fraction (c) for single- and dual-grid RRLES of the TRZ flame.

at different levels of initial turbulence intensity and analyze flame-turbulence interactions. The strengths and weaknesses of both strategies are assessed by comparison with DNS data.

Overall, both strategies capture the flame structure in reasonable agreement with the DNS data but with some slight variations in quantitative predictions. The single-grid RRLES tends to under-predict all spatially and conditionally averaged quantities while the dual-grid RRLES appears to slightly over-predict. This could be explained by the dual-grid strategy having more unresolved scales available at the subgrid LEM level.

ACKNOWLEDGMENTS

The computational resources for this study are provided by the Center of Excellence in Applied Computational Science and Engineering at UTC. Dr. Ranjan would also like to acknowledge the support from NSF (Grant #: 2301829, Program Officer: Dr. Harsha Chelliah).

REFERENCES

- [1] Aspden, A. J., Day, M. S., and Bell, J. B., (2011) "Turbulence-flame interactions in lean premixed hydrogen: transition to the distributed burning regime," *J. Fluid Mech.*, 680, pp. 287–320.
- [2] Boger, M., Veynante, D., Boughanem, H., and Trouve, A., (1998) "Direct numerical simulation analysis of flame surface density concept for large eddy simulation of turbulent premixed combustion," *Proc. Combust. Inst.*, 27, pp. 917–925.
- [3] Bowers, J., Durant, E., and Ranjan, R., (2021) "Application of intrusive and non-intrusive reduced order modeling techniques for simulation of turbulent premixed flames," *AIAA Propulsion and Energy 2021 Forum*, p. 3634.
- [4] Colin, O., Ducros, F., Veynante, D., and Poinsot, T., (2000) "A thickened flame model for large eddy simulations of turbulent premixed combustion," *Phys. of Fluids*, 12(7), pp. 1843–1863.
- [5] Colucci, P., Jaberi, F., Givi, P., and Pope, S., (1998) "Filtered density function for large eddy simulation of turbulent reacting flows," *Phys. of Fluids*, 10(2), pp. 499–515.
- [6] Echekki, T., Kerstein, A. R., Dreeben, T. D., and Chen, J.-Y., (2001) "?one-dimensional turbulence? simulation of turbulent jet diffusion flames: model formulation and illustrative applications," *Comp. and Fluids*, 125(3), pp. 1083–1105.
- [7] Fox, R. O. and Raman, V., (2004) "A multienvironment conditional probability density function model for turbulent reacting flows," *Phys. of Fluids*, 16(12), pp. 4551–4565.
- [8] Fureby, C., (2009) "Large eddy simulation modelling of combustion for propulsion applications," *Philosophical Transactions of the Royal Society A: Mathematical, Physical and Engineering Sciences*, 367(1899), pp. 2957–2969.
- [9] Gao, F. and O'Brien, E. E., (1993) "A large-eddy simulation scheme for turbulent reacting flows," *Phys. of Fluids*, 5, pp. 1282–1284.
- [10] Génin, F. and Menon, S., (2010) "Studies of shock/turbulent shear layer interaction using Large-Eddy Simulation," *Computers & Fluids*, 39, pp. 800–819.
- [11] Goodwin, D. G., Moffat, H. K., and Speth, R. L., (2014) "Cantera: An object-oriented software toolkit for chemical kinetics, thermodynamics, and transport processes,", http://www.cantera.org, version 2.1.2.
- [12] Kerstein, A. R., (1989) "Linear-eddy modeling of turbulent transport. II: Application to shear layer mixing," *Combust. Flame*, 75(3-4), pp. 397–413.
- [13] Kim, W. W. and Menon, S., (1999) "An unsteady incompressible Navier-Stokes solver for large eddy simulation of turbulent flows," *I. J. for Numer. Meth. Fluids.*, 31(6), pp. 983–1017.
- [14] Kim, W.-W. and Menon, S., (2000) "Numerical modeling of turbulent premixed flames in the thin-reaction-zones regime," *Combust. Sci. Technol.*, 160(1), pp. 119–150.
- [15] Klimenko, A. Y. and Bilger, R. W., (1999) "Conditional moment closure for turbulent combustion," *Prog. Energy Combust. Sci.*, 25(6), pp. 595–687.
- [16] Lowery, C., Hasti, V. R., and Ranjan, R., (2022) "Characteristics of non-equilibrium turbulence in couette flow under compressible conditions," *AIAA AVIATION 2022 Forum*, p. 4035.
- [17] MacCormack, R. W., (2003) "The effect of viscosity in hypervelocity impact cratering," J. Space. Rockets, 40(5), pp. 757–763.
- [18] Menon, S. and Kerstein, A. R., (2011) "The linear-eddy model," Turbulent Combustion Modeling, 95, pp. 175–222.
- [19] Menon, S. and Kim, W., (1996) "High Reynolds number flow simulations using the localized dynamic subgrid-scale model," *AIAA paper*, 425, pp. 1996.

- [20] Menon, S., McMurtry, P., and Kerstein, A. R., (1993) "A linear eddy mixing model for large eddy simulation of turbulent combustion,", *LES of Complex Engineering and Geophysical Flows*. Galperin, B. and Orszag, S. (Eds.). Cambridge University Press, pp. 287–314.
- [21] Menon, S. and Patel, N., (2006) "Subgrid modeling for simulation of spray combustion in large-scale combustors," *AIAA J.*, 44, pp. 709–723.
- [22] Panchal, A., Ranjan, R., and Menon, S., (2019) "A comparison of finite-rate kinetics and flamelet-generated manifold using a multiscale modeling framework for turbulent premixed combustion," *Combustion Science and Technology*, 191(5-6), pp. 921–955.
- [23] Peters, N., (2000) Turbulent Combustion, Cambridge University Press.
- [24] Pitsch, H., (2006) "Large-eddy simulation of turbulent combustion," Annu. Rev. Fluid Mech., 38, pp. 453-482.
- [25] Poinsot, T. and Veynante, D., (2005) Theoretical and Numerical Combustion, 2nd Edition, Edwards, Inc.
- [26] Poludnenko, A. Y. and Oran, E. S., (2011) "The interaction of high-speed turbulence with flames: global properties and internal flame structure," *Combust. Flame*, 157(5), pp. 995–1011.
- [27] Ranjan, R., (2021) "A dual grid strategy for subgrid reaction-rate closure using linear eddy mixing model for large-eddy simulation of turbulent combustion," *APS Division of Fluid Dynamics Meeting Abstracts*, pp. H09–003.
- [28] Ranjan, R., Muralidharan, B., Nagaoka, Y., and Menon, S., (2016) "Subgrid-scale modeling of reaction-diffusion and scalar transport in turbulent premixed flames," *Combust. Sci. Technol.*, 188, pp. 1496–1537.
- [29] Sankaran, R., Hawkes, E. R., Chen, J. H., Lu, T., and Law, C. K., (2007) "Structure of a spatially developing turbulent lean methane–air Bunsen flame," *Proc. Combust. Inst.*, 31(1), pp. 1291–1298.
- [30] Sankaran, V. and Menon, S., (2005) "Subgrid combustion modeling of 3-D premixed flames in the thin-reaction-zone regime," *Proc. Combust. Inst.*, 30(1), pp. 575–582.
- [31] Savre, J., Carlsson, H., and Bai, X. S., (2013) "Turbulent methane/air premixed flame structure at high Karlovitz numbers," *Flow Turbulence Combust.*, 90(2), pp. 325–341.
- [32] Steiner, H. and Bushe, W., (2001) "Large eddy simulation of a turbulent reacting jet with conditional source-term estimation," *Phys. of Fluids*, 13(3), pp. 754–769.
- [33] Trouve, A. and Poinsot, T., (1994) "The evolution equation for the flame surface density in turbulent premixed combustion," *J. Fluid Mech.*, 278, pp. 1–31.
- [34] Vreman, B., Geurts, B., and Kuerten, H., (1994) "On the formulation of the dynamic mixed subgrid-scale model," *Phys. of Fluids*, 6, pp. 4057–4059.
- [35] Wang, H., Hawkes, E. R., Chen, J. H., Zhou, B., Li, Z., and Aldén, M., (2017) "Direct numerical simulations of a high Karlovitz number laboratory premixed jet flame—an analysis of flame stretch and flame thickening," *J. Fluid Mech.*, 815, pp. 511–536.
- [36] Yang, S., Ranjan, R., Yang, V., Wenting, S., and Menon, S., (2017) "Sensitivity of predictions to chemical kinetics models in a temporally evolving turbulent non-premixed flame," *Combustion and Flame*, 183, pp. 224–241.
- [37] Yuen, F. and Gülder, Ö. L., (2009) "Investigation of dynamics of lean turbulent premixed flames by Rayleigh imaging," *AIAA J.*, 47(4), pp. 2964–2973.